**Proceedings of the ASME 2021 16th International Manufacturing Science and Engineering Conference MSEC2021
June 21-25, 2021, Virtual, Online**

MSEC2021-63351

DISCRETE-ELEMENT SIMULATION OF POWDER SPREADING PROCESS IN BINDER JETTING, AND THE EFFECTS OF POWDER SIZE

Ana Paula Clares[1], Dr. Guha Manogharan[1,2*]
[1]Additive Manufacturing & Design Graduate Program,
[2]Department of Mechanical Engineering,
The Pennsylvania State University.
University Park, PA
*Corresponding author: gum53@psu.edu

ABSTRACT

Binder Jetting has gained particular interest amongst Additive Manufacturing (AM) techniques because of its wide range of applications, broader feasible material systems, and absence of rapid melting-solidification issues present in other AM processes. Understanding and optimizing printing parameters during the powder spreading process is essential to improve the quality of the final part. In this study, a Discrete Element Method (DEM) simulation is employed to evaluate the powder packing density, flowability, and porosity during powder spreading process utilizing three different powder groups. Two groups are formed with monoidal size distributions (75-84 µm and 100-109 µm), and the third one consisting of a bimodal distribution (50 µm +100 µm).

A thorough investigation into the effects of powder size distribution during the powder spreading step in a binder jetting process is conducted using ceramic foundry sand. It was observed that coarser particles result in higher flowability (62% decrease in repose angle) than finer ones due to the cohesion effect present in the latter. A bimodal size distribution yields the highest packing density (8% increase) and lowest porosity (~12% reduction) in the powder bed, as the finer particles fill in the voids created between the coarser ones. Findings from this study are directly applicable to binder-jetting AM process, and also offer new insights for AM powder manufacturers.

Keywords: additive manufacturing, ceramics, binder jetting, powder size, porosity, layer density, flowability.

NOMENCLATURE

a	acceleration (m/s)
D	roller diameter (cm)
d	diameter (µm)
f	packing fraction adjustment
F	total force between particles (N)
F_c	contact force (N)
F_e	elastic force (N)
F_n	force in normal direction (N)
F_t	force in tangential direction (N)
H	roller height (cm)
k	spring constant
K	bonding number
m	mass of particle (g)
P	particles required
r	radius (cm)
u	relative velocity (m/s)
v	particle velocity (m/s)
V_d	domain volume (cm^3)
V_{total}	total cavities present (cm^3)
V_{wp}	wall-particle cavity volume (cm^3)
x	particle
γ	surface energy (N/m)
δ	displacement (cm)
η	damping coefficient
g	gravity (cm/s^2)
y	moving distance (cm)
ρ	density (g/cm^3)

1. INTRODUCTION

Additive manufacturing (AM) has gained significant popularity due its ever-growing capabilities to join materials layer by layer based on three-dimensional (3D) model data [1], offering a wide array of applications [2], [3]. Among the several recent advancements in AM, powder bed-based processes have garnered significant attention due to their finer resolution, higher part quality, powder reusability [4], and functional parts [5]. This study focuses on binder jetting, a process in which a liquid binding agent is selectively deposited to join powder materials [6].

Among the seven AM processing categories [7], binder jetting has gained a spotlight of its own, as the process is one of the most promising techniques to work with ceramic materials [6]. Because of their physical properties, ceramics cannot be easily cast or machined and hence, AM offers a viable technology for production of ceramic parts with higher geometrical complexity [8]. Ceramics offer unique characteristics, such as biocompatibility, hardness, and resistance to wear, heat, and corrosion [9], which are ideal for aerospace [10], [11], biomedical [12]–[14], and other applications [15], [16]. Although ceramic binder jetting is a relatively simpler AM process which does not require expensive lasers or electron beam, additional steps for post-printing such as de-powdering, curing, de-binding, and sintering are necessary to achieve a fully dense part.

Since binder jetting is a powder bed-based technology, it is essential to understand the underlying physics of powder particles during the spreading process which has a significant impact on the characteristics and quality of the final product [17], [18]. Binder jetting employs a relatively larger powder size distribution (when compared with other AM technologies [19], [20]) which requires post-processing to achieve non-porous fully dense parts [21]. Bai et al. [21] demonstrated an improvement in powder packing density and flowability (10.5% increase) through the use of bimodal powder size distribution in copper powders. Chen et al. [22] evaluated a counter-rolling powder spreading process and the effects of spreading speed. It was found that a higher spreading speed reduced the packing density because of increase in particle's moving strength which lowered the mass flow rate. However, this phenomenon is further amplified in bimodal particle size distribution which is investigated in this paper for better understanding.

Because of the significant time and cost implications of full factorial experimental investigations of the powder spreading process in AM, numerical simulations such as the discrete element method (DEM) have manifested as an effective way to replicate the spreading process at a particle scale [6], [23]–[26]. Many investigations based on DEM have focused on predicting layer density and resulting mechanical strength [26], [27]. Miao et al. [6] employed the DEM in ceramic binder jetting to simulate the powder spreading process to predict powder bed density and study the influence of layer thickness and roller diameter. This study highlighted the need to further research the effects of particle size distribution in binder-jetting. Similarly, Lee et al. [28] developed a DEM model to understand the powder packing dynamics in AM with varying size distributions. This study noted that a mix of powder diameters results in an improvement of packing density.

Du et. al's study [29] is based on analytical modeling and experimental methods to optimize powder ratios for the highest tap density in a silicon carbide ceramic part. The results highlighted the use of a modeling method to predict the tap density of bimodal powders with high accuracy. Similar outcomes were found by Bai et. al [30], where bimodal mixtures led to improved apparent and tap densities across several material systems. The study observed improvements in powder bed density, and sintered density with the introduction of the bimodal distributions. Other works, however, such as in [31], found bimodal mixing to be potentially detrimental, as they may decrease the ultimate tensile strength based on the material system (e.g., copper). Chen et al. [23] did not observe any effects of bimodal distributions in stainless-steel powders during powder spreading process as they hypothesize that percolation effect has stronger influence on the overall process. Nevertheless, the authors recommended investigating different materials and different combinations of bimodal mixtures to evaluate the impact of powder size distributions on packing density. In summary, reported findings are primarily focused only on metallic materials which are produced via atomization and have highly different physical and morphological properties when compared with ceramics. Since binder-jetting is extensively used in ceramics [32], there is a critical need for an investigation about the impact of multimodal distributions in ceramic feedstock during the powder spreading process.

This original research aims to quantitively investigate the fundamental impact of powder size distribution in ceramics on powder bed packing density, porosity, and flowability in a binder jetting process through DEM simulation techniques. Our empirical results validate that the use of bimodal sized distributions enhances the flowability and packing density of a powder spreading process. An increase in flowability between finer particles and bimodally distributed ones was reflected by a 49% reduction in the angle of repose between the finer size distributions used and the bimodal ones. In addition, an 8% increase in packing density was observed in the bimodal ceramic powder size distribution.

The rest of the paper is organized as follows. Section 2 describes an overview of the binder jetting process with a focus on the powder spreading and deposition mechanisms. Section 3 and 4 detail the material and selection of powder size distributions. In Section 5, the methodology and parameters used in the DEM simulations are presented. Sections 6 highlights the major results and analysis from this study, along with a summary of major conclusions, limitations and future direction for this research in Section 7.

2. METHODS

2.1 Binder Jetting Process

This section details the binder jetting AM process shown in *Figure 1*. First, a desired quantity of the powder is fed to the spreading roller (feed to powder ratio varies from 1 to 3) which evenly distributes a layer of powder across the powder bed in the build chamber. Subsequently, radiation from heat lamps is applied to remove moisture prior to binder deposition. Lastly, the array of nozzles in the printhead selectively deposits, i.e., jets droplets of binder onto the powder bed based on the three-dimensional (3D) model of the printed part. This binder will act as an adhesive, joining the powder particles together due to surface tension created by the binder. This process is repeated layer by layer by lowering the build platform after each powder spread, until the final part is printed.

After the fabrication process is concluded, the part is carefully removed from the build platform acting as a "green part," which refers to the printed part's initial state without the final mechanical conditions achieved by post-AM processing [33]. Upon removal from the build platform, the "green part" undergoes de-powdering, curing, de-binding, sintering, consolidation, and infiltration [6], [33] depending on the build material, to achieve the final part properties. For instance, in the case of 3D sand-printing, the sand molds and cores produced via binder-jetting can be used without any additional post-processing [34]–[36].

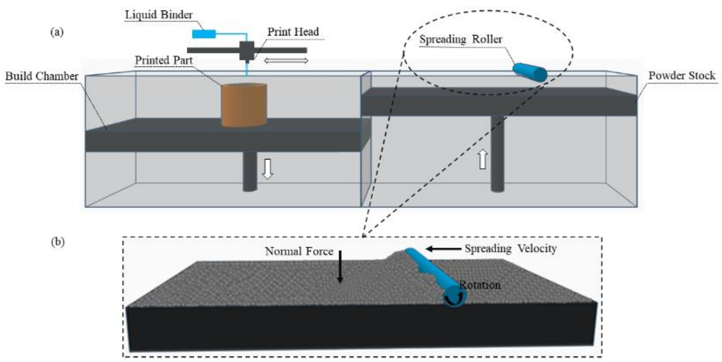

Figure 1:*a)Binder jetting additive manufacturing (AM) set-up. b)Forces in the powder spreading process.*

2.2 Spreading and Deposition Mechanisms

In powder bed based AM processes, the powder deposition and spreading stage plays an essential part in the layer's packing density, determining the final part's quality [22]. Based on a prior study, three types of deposition mechanisms have been identified in the powder spreading process [23]: namely, the wall effect, cohesion effect, and percolation effect which can be mitigated to achieve a better packing density.

The wall effect influences the presence of cavities near the base plate during powder deposition in the initial several layers of the build process. As the powder is being spread, the roller acts as a wall restraining the free movement and deposition of particles [23], and is represented in Eq. (1) based on the volume ratio between the wall-particle cavities V_{wp} and total cavities present V_T. Larger volume ratio indicates presence of stronger wall effect. The particle's diameter, roller diameter, and roller height are represented by d, D, and H, respectively:

$$V_{wp} = \frac{1}{6}\Pi^2 \, dD\frac{D}{4} + H \qquad (1)$$

$$V_T = 0.4\pi\frac{D^2}{4}\frac{H+1}{6\Pi^2 d}D \cdot \frac{D}{4+H}$$

where

$$\frac{V_{wp}}{V_T} = \frac{d\left(\frac{1}{H}+\frac{4}{D}\right)}{0.8+d\left(\frac{1}{H}+\frac{4}{D}\right)}$$

This study suggested that higher powder layer thickness could reduce the wall effect [23].

The cohesion effect due to van der Waals force causes agglomerations in the powder packing process before spreading. The simplified formula presented in Eq. (2), is used to evaluate the influence of van der Waals forces. The ratio of van der Waals forces between two spherical particles and gravity is represented by the bonding number, K.

$$K = \frac{3\pi\gamma}{8}d = \frac{9\gamma}{4\rho g} \cdot \frac{1}{d^2} \qquad (2)$$

γ , d, ρ, and g represent the material's surface energy, particle diameter, material's density, and gravity employed in the study. Since the bonding number is inversely proportional to the particle diameter, a decrease in particle size will result in higher van der Waals forces, leading to particle agglomeration. It is recommended to identify an optimal "inflection point" of particle size diameter that will lower the K number [23].

Finally, the percolation effect causes the powder particles to collide with each other as they pass through the moving powder bed in monoidal powder size distributions. In bimodal distributions, this effect could lead to powder segregation, since cavities could result from finer particles traveling faster than coarser particles in the powder bed.

Several process parameters are currently being investigated to improve the performance of binder jetting parts and reduce defects such as particle jamming, porosity, and formation of cavities [25]. Another study has shown that applying a mechanical load such as normal stress on the powder, normal stress on the roller, and friction stress have an impact on the powder spreading process [6]. Chen et al. use DEM to evaluate the influence of particle contact stress and particle velocity mechanical properties [23]. Other studies have focused on the influence of particle size distributions and particle shape to understand their impact on the spreading process [24], [25], [37].

However, there is a major knowledge gap in the literature on the critical impact of the type of spreader, coupled with a rotational and translational speed on the quality of powder deposition. Different powder-spreading methods are used to deposit the powder onto the baseplate, but the most common spreader systems are based on scrapes and rollers. A recent study illustrated the benefits of concurrently using both counterclockwise roller and a spreader [37]. In the study, the rake yielded better packing results and fewer part-shifting defects than a counter roller in finer particle size distributions.

Although a uniform powder layer might not always be achievable in a spreading process, results using a rake with a spreader speed of 100 mm/s, have shown that the inconsistent powder pile size does not directly affect the packing density of the bed [23].

Other studies based on particle spread simulations have used a counterclockwise rotating roller to analyze the effect of spreading speed on powder bed. It was found that an increase in the roller's velocity will increase the surface roughness of the layers as well [26]. Finally, counter-rolling powder spreading resulted in a decrease in packing density and poor surface quality of the powder layers with increase in spreading speed [22].

3. MATERIALS

The feedstock material used in this research was powdered ceramic foundry sand, *Cerabeads®* consisting of Al_2O_3 61% and SiO_2 36% [38]. The material was chosen for its excellent manufacturing, mechanical, and chemical properties and relevance for 3D Sand-Printing for sand-castings [35], [39]. The ceramic sand's spherical morphology offers an increase in flowability which directly impacts the quality of the powder bed [9].

This material has been growing in its applications across different industries such as automotive, oil and gas, mining, and construction because of its higher strength, higher heat resistance, improved part resolution, improved surface finish, reduced waste, stable grain size distribution, and high refractoriness [38]. Additional benefits that make this material ideal for binder-jetting is its lower thermal expansion, high durability, and low thermal conductivity.

Although limited reported studies have focused on processing ceramic sand via AM technologies, few studies demonstrate the benefits of using binder jetting for rapid printing of sand-casting molds [40], [41] and other applications.

4. POWDER SIZE

Based on specifications required for binder-jetting of ceramic foundry sand, powder size distributions are selected to evaluate their performance on porosity, powder packing density, and flowability in the DEM simulation.

A prior study demonstrated that particle size distribution highly impacts on achieving a high maximum packing density and uniform layer in a powder spreading process [24]. A ceramic sand's size distribution ranging from 50-109 μm and a powder bulk density of 1.69 g/cm^3 is chosen, and grouped into different categories to analyze its effect on the spreading process, as shown in *Table 1*. Ceramic foundry spherical particles are considered in this study because of their desired flowability properties and filling efficiencies [9], [38].

Table 1: *Particle size distributions classified into three groups.*

Group	Particle Size Distribution (μm)	Mean Particle Size (μm)	St. Dev. of particle size (μm)
1	75-84	79.5	2.87
2	50+100	66	-
3	100-109	104.5	2.87

Three different groups corresponding to a range of powder sizes were selected for the analysis of results. Group 1 has a uniform distribution of powders ranging from 75-84 μm with a mean particle size of 79.5 μm. This group was selected because of the advantage of finer particles during sintering [9]. In group 2, the coarse to fine mass ratio of 1:3 in the bimodal size distributions is considered in the design of experiments based on calculation from combining particles of 50 μm and100 μm [21], [23].

In recent years, there is a growing interest in quantifying the effect of monoidal or multimodal powder size distributions [9], [21], [24] in powder spreading processes in AM. The motivation for multimodal distributions lies in the postulation that it could increase powder packing density such that finer particles fill the created voids by coarser particles. This filling effect is presented in *Figure 2* (finer particles in green fills the voids formed between the coarser particles in red). As the ratio of finer to coarser particles increases, it is necessary to avoid the loosening effect that results from overfilling the created voids [17].

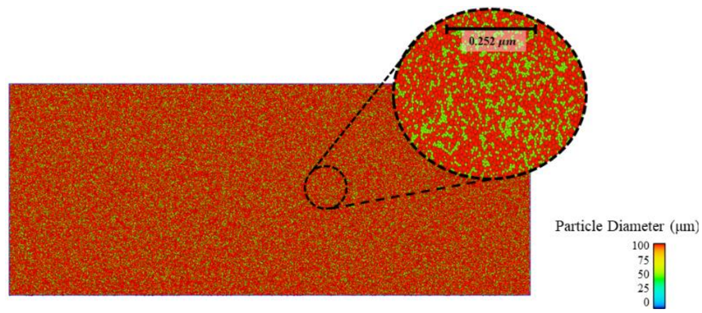

Figure 2: *Top view (xy plane) of the DEM generated powder bed illustrates the filling effect in bimodal powder distribution with coarser (100 μm in red), and finer (50 μm in green) particles.*

This could increase powder bed layer density, flowability, and hence the green density of a printed part, [9], [17], [21]. However, determining an appropriate particle gradation is a necessary step prior to part fabrication which could be achieved by varying particle mixtures of finer to coarser ratios based on trial-and-error [42], a model-guided selection [9], Furnas model [43], and linear packing models [44].

Finally, group 3 has a uniform distribution of powders ranging from 100-109 μm with a mean value of 104.5 μm. The coarse particles were selected because of their favorable higher flowability. The layer height (μm) of each corresponding group is equal to about two times the largest powder size diameter (μm) of that group to ensure smooth spreading of the powder layer [23]. Groups 1, 2, and 3 have layer heights of 170, 200, and 220 μm, respectively.

5. SIMULATION

The DEM simulation setup, calculations and parameters used are presented in this section.

5.1 Discrete Element Method

The powder spreading process in a binder jetting system (e.g., ExOne Innovent+) is simulated with FLOW-3D CFD software (Release 3 version, Flow Science, Santa Fe, NM, USA) based on DEM methodology. DEM is a numerical method to solve Newton's equation of translational and rotational motions by analyzing impact forces and dynamic interaction between powder particles by tracking the movements and inter-collisions of powder particles as discrete and rigid bodies.

The DEM solves the fundamental equation of motion represented in Eq. (3), where the force of particle i is calculated (mass of a solid particle m_i multiplied by the acceleration of a_i) for all contact forces due to particle interaction F_C and the external force, and gravity g. The sum of contact forces only corresponds to the particles in direct contact with the ith particle.

$$m_i a_i = \Sigma F_C + g \tag{3}$$

Since particle-particle interactions have multiple forces acting upon them, a spring-damper model is applied for the elastic forces and viscous dissipation based on the Voigt Model, which considers the contact in a normal and tangential direction. Eq. (4) is used to calculate the elastic force in DEM as a linear spring following Hooke's law, and elastic force F_e is calculated using a spring constant k and displacement δ.

Consequently, the displacement between particles δ_{ij} is calculated based on Eq. (5), with distance L_{ij} between the center coordinates x_i and x_j of both interacting particles.

$$F_e = -k\delta \tag{4}$$

$$\delta_{ij} = L_{ij} - \left(r_i + r_j\right) \tag{5}$$

$$L_{ij} = \left\|x_i - x_j\right\|$$

The total force between particles in the DEM model F_i is calculated based on the sum of the forces in normal direction F_n and the force in the tangential direction F_t as shown in Eq. (6).

$$F_i = F_n + F_t \tag{6}$$

$$F_n = -k_n \delta_{n_ij} - \eta_n u_{n_ij} \tag{7}$$

$$F_t = -\eta_t u_{tij} \tag{8}$$

In Eq. (7), the normal component F_n is calculated from k_n, $\delta_{n_ij}, \eta_n, u_{n_ij}$, which correspondingly represent spring constant in the normal direction, displacement between the solid particles i and j, damping coefficient in the normal direction, and relative velocity between solid particles i and j. In Eq. (8), the tangent component F_t uses η_t and u_{tij} as the damping coefficient along the tangent, and relative velocity between solid particles i and j.

5.2 Simulation Setup

The DEM simulation setup presented in *Figure 3* is generated for a representative build box with corresponding length (4 cm), height (1.625 cm), and width (1.625 cm) in the *xyz* coordinate system. The boundaries of the model are treated as wall boundaries, with an exception at the outflow side (left end in *Figure 3*) to allow for flow of particles to exit the system after spreading by a roller (4 cm in diameter and 0.25 cm in length). The dimensions in this DEM study mimic the build box of a commercially available binder jetting printer but are scaled down by a factor of 4 to lower computational costs.

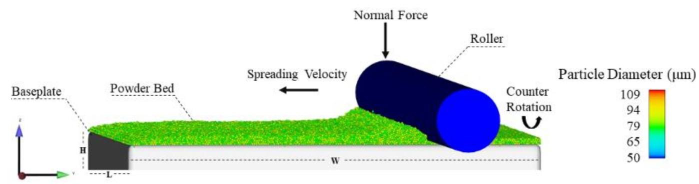

Figure 3: *Schematic of the powder spreading simulation setup (e.g., powder size distribution:75-84 µm).*

The simulation process begins with randomly generated particles that are settled into the print bed. After this, the spreading process begins with a counter-clockwise rotating roller that spreads the fine powder, to form a thin layer along the *-y* direction. The appropriate layer height utilized for each simulation group was calculated based on powder size as detailed in Section 4. The number of particles required for each simulation, based on their group number, are calculated using Eq. (9), where P, v_d, and f are number of particles required in the simulation, domain volume, and packing fraction adjustment.

$$P = \frac{v_d}{f} \tag{9}$$

Additional parameters employed DEM simulation are presented in *Table 2.* The density of the material, Young's modulus, and Poisson ratio correspond to the ceramic foundry sand studied. It should be noted that the coefficient of friction is critical in DEM studies since it directly impacts the dynamic behavior of powder particles [33].

Table 2: *Parameters used in the DEM simulation setup.*

Parameters	Value	Unit
Material's density (ρ) [38]	1.69	g/cm^3
Young's modulus (E)	1.55E+11	GPa
Poisson ratio (η)	0.18	
Restitution coefficient [45], [46]	0.9	
Friction coefficient [47] (dynamic, static)	(0.27, 0.19)	
Spring constant (k)	9.72E+02	
Gravity (g)	980	cm/s^2

The coefficient of restitution (COR) for this simulation was selected based on previous work [45], [46]. An investigation on the effect of the COR of silica sand [45] using different COR values yielded a value of 0.9 for the dry ceramic sand. The COR will increase at higher spreading velocity. Another study [46] that investigated glass spheres on vertical dispensing hoppers yielded similar results for COR value ranging from 0.9-0.94 for particle collisions.

During powder spreading process, an additional phenomenon that should be considered is slipping due to the contact boundary condition which imposes relative velocity between bodies under contact with each other. In this case, it is critical to account for this effect because of its impact on the quality of the spread layers and subsequently, the final print quality. Studies [48], [49] performed to improve layer quality have suggested the avoidance of excessive slip by inducing higher particle-wall frictions.

The DEM model uses the simplified Hertz Mindlin model that includes nonlinear elastic and slip [50], [51]. In this simulation study, two spring-damper models are created for normal contact between particle-wall interactions, and tangential (rolling friction) contact. In addition, slipping is accounted in the simulation setup. The parameter for slip ranges from 0 to 1 with 1 reflecting no slip on the contact surface [51], and every value in between displaying a partial slip with increasing effects along radial inward direction from the edge of the contact area, i.e. at slip-stick region [51]. In this study, the parameters for partial slip are calculated from the particle-wall friction coefficient which accounts for the interaction between the powder and roller.

The spring constant k of the spherical shapes is calculated in Eq. (10) for all the three groups in this study. In this equation, ρ, d, v, are the particle's density, maximum particle diameter in the corresponding group, and particle velocity that can be calculated with Eq. (11), respectively, where y is the moving distance.

$$k = 10 \frac{\rho v^2 \pi d^3}{6\left(\frac{d}{2}\right)^2} \tag{10}$$

$$v = 2\sqrt{2gy} \tag{11}$$

6. SIMULATION RESULTS AND DISCUSSION

In this section, the results from the DEM simulation are presented by highlighting the three critical powder spreading parameters studied to achieve higher-quality in binder-jetting AM parts.

6.1 Powder Packing Density and Porosity

The bulk volume and powder weight after spreading runs were used to estimate the powder packing density as shown in *Figure 4.* A close-up view of the bounding box is presented at the top right of each figure to illustrate powder packing. The clearly visible piling on the powder bed in *Figure 4* across all three groups at the same time stamp is caused by roller spreading, which is not presented for visualization.

In order to account for process variance, three measurements of the packing density were taken per group size (*Table 3*). *Table 4* presents a one-way analysis of variance (ANOVA) as recommended by ASTM E2655. Referring to the calculated analysis of *Figure 4*, there is statistically significant influence of powder size distribution on packing density at a 95% confidence interval. The average final powder packing densities of groups 1, 2, and 3 are 60%, 64%, and 59%, respectively. It is observed that a bimodal size distribution has an increase in packing density when compared to the monoidal sized groups. This phenomenon occurs due to cohesion of finer mono sized particles, and wall effect that is present in larger particle diameters.

Results from this study are in agreement with reported findings [21], where bimodal mixture increased the powder packing density by 8.2%. Bai et al. [30] also found an improvement on apparent (12.7%) and tap density (5.6%) with the introduction of the bimodal powder size distributions.

Table 3*:Powder packing densities measurements.*

Groups	Count	Sum	Average	Variance
group 1	3	1.8	0.6	0.0004
group 2	3	1.92	0.64	0.0001
group 3	3	1.77	0.59	0.0004

Table 4: *Statistical tests show significant effects of powder size distributions on packing density at 95% confidence level.*

Source of Variation	SS	df	MS	F	p-value	F_{crit}
Between groups	0.0042	2	0.0021	7	0.027	5.143253
Within groups	0.0018	6	0.0003			
Total	0.006	8				

Porosity has often been associated with density in a powder spreading process [9]. It is a measure of void spaces that are created in the powder bed and is widely present in ceramic binder jetting [15]. Porosity (in percentage) of the powder layer is calculated using FlowSight (Particle STL converter software) and as expected, bimodal group 2 has the lowest porosity of 36%. Group 1 has a porosity of 40%, which is closer to the bimodal sized powder, and group 3 of 41%. This could be attributed to the formation of voids during particle-wall interactions between particle-print bed and particle-roller [48], [52] which causes agglomerations during the powder spreading process.

6.2 Powder Flowability

The angle of repose (AOR) as shown in *Figure 5* is calculated at the same timestamp to measure flowability from the steepest angle of descent formed during the powder spreading process with respect to the previous layer. The AOR results achieved for group 1, group 2, and group 3 were 34.45°, 17.23°, and 13.14°, respectively. A smaller angle of repose has been shown to result in higher flowability [53]. It can be observed that although the coarser and bi-modal powder sizes yield a lower angle of repose, the overall high flowability of the group sizes can be attributed to the spherical shape [21]. In addition, the use of only finer particles engage in a stronger cohesion effect during spreading which increases the van der Waals force and tends to form agglomerates with poor flowability [9], [24], [53]. This agrees with results obtained by Bai et al., where powder flowability increased by 9.4% in bi-modal powder size distribution [21]. Overall, the results present a promising path for improving flowability during powder spreading in binder jetting AM process to achieve smooth and dense layers [21].

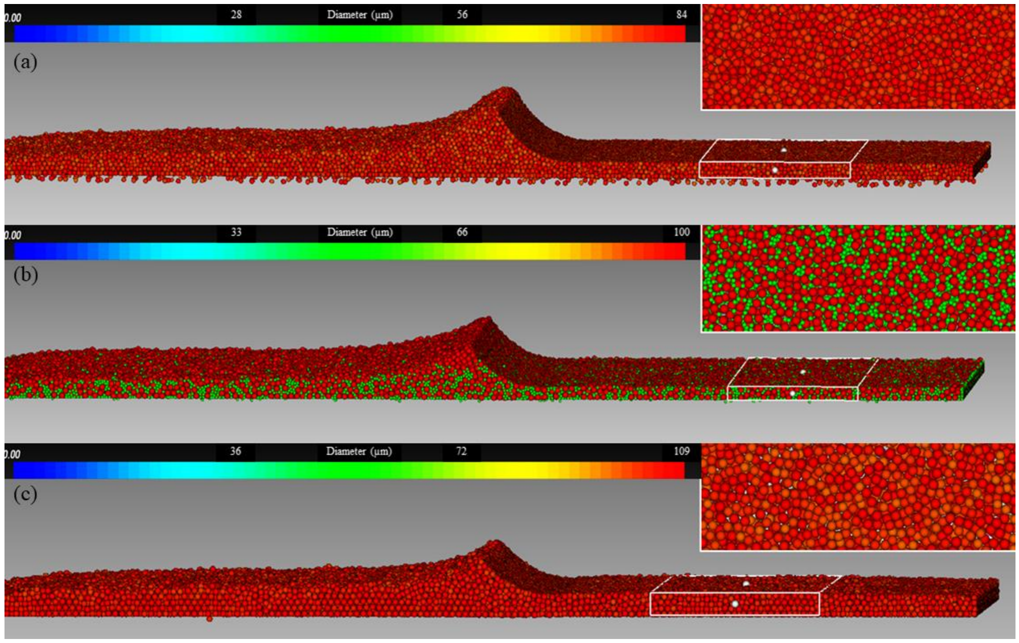

Figure 4: Powder packing density at 0.53 seconds for powder size distributions: a) 75-84 μm b) 50+100 μm c) 100-109 μm.

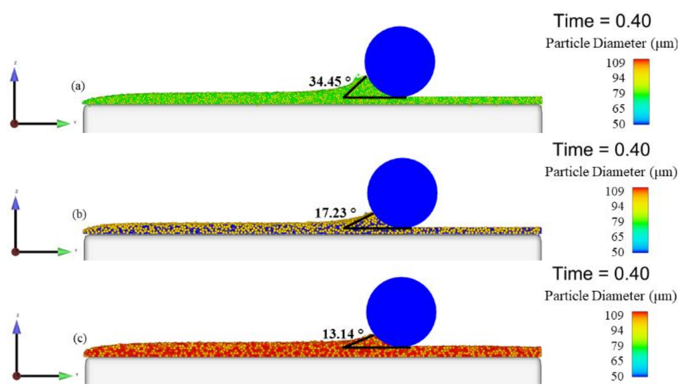

***Figure 5:** Angle of repose at 0.40 seconds for powder size distributions: a) 75-84 μm b) 50+100 μm c) 100-109 μm.*

7. CONCLUSION

Powder size distribution selection has a major impact on enhanced mechanical and physical properties for fabricated binder jetted parts. This paper presents a discrete element model (DEM) computational study to investigate packing density, powder bed porosity, and flowability of ceramic sand in binder-jetting AM processes. Based on the results and analysis, we report the following major findings:

- Coarser particles have higher flowability values when compared with finer particles with higher resistance to particle agglomeration. Although, finer particle distribution can be beneficial for higher sinterability and require post-processing techniques like infiltration to reduce porosity in the final AM part.
- Bimodal size distribution can increase powder packing density and lower porosity.

Future work will include further exploration of the use of bimodal size distribution and selecting of different ratios of particle sizes to see the effect on the printed part's quality. Experimental validation is currently pursued by the authors using a binder jet (Innovent+) to investigate the underlying effect of cohesive response in bimodal particle distributions.

ACKNOWLEDGEMENTS

The author acknowledges the support from 2020 PA Manufacturing Fellows Initiative Grant, NSF CMMI award# #1944120, Flow Science, The Pennsylvania State University, and ExOne. Special thanks to Tess Zangrilli from Flow Science for her support.

REFERENCES

[1] B. Mansfield, S. Torres, T. Yu, and D. Wu, "A review on additive manufacturing of ceramics," in *ASME 2019 14th International Manufacturing Science and Engineering Conference, MSEC 2019*, Nov. 2019, vol. 1, doi: 10.1115/MSEC2019-2886.

[2] E. O. Olakanmi, R. F. Cochrane, and K. W. Dalgarno, "A review on selective laser sintering/melting (SLS/SLM) of aluminium alloy powders: Processing, microstructure, and properties," *Progress in Materials Science*, vol. 74. Elsevier Ltd, pp. 401–477, Aug. 01, 2015, doi: 10.1016/j.pmatsci.2015.03.002.

[3] L. Yang and H. Miyanaji, "Ceramic additive manufacturing: a review of current status and challenges."

[4] T. D. Ngo, A. Kashani, G. Imbalzano, K. T. Q. Nguyen, and D. Hui, "Additive manufacturing (3D printing): A review of materials, methods, applications and challenges," *Composites Part B: Engineering*, vol. 143.

Elsevier Ltd, pp. 172–196, Jun. 15, 2018, doi: 10.1016/j.compositesb.2018.02.012.

[5] S. A. Khairallah, A. T. Anderson, A. Rubenchik, and W. E. King, "Laser powder-bed fusion additive manufacturing: Physics of complex melt flow and formation mechanisms of pores, spatter, and denudation zones," *Acta Mater.*, vol. 108, pp. 36–45, Apr. 2016, doi: 10.1016/j.actamat.2016.02.014.

[6] G. Miao, W. Du, and Z. Pei, "Binder jetting additive manufacturing of ceramics: Analytical and numerical models for powder spreading process," in *ASME 2019 14th International Manufacturing Science and Engineering Conference, MSEC 2019*, Nov. 2019, vol. 1, doi: 10.1115/MSEC2019-2925.

[7] "ASTM E2655 - 14(2020) Standard Guide for Reporting Uncertainty of Test Results and Use of the Term Measurement Uncertainty in ASTM Test Methods." https://www.astm.org/Standards/E2655.htm (accessed Feb. 14, 2021).

[8] Z. C. Eckel, C. Zhou, J. H. Martin, A. J. Jacobsen, W. B. Carter, and T. A. Schaedler, "Additive manufacturing of polymer-derived ceramics," *Science (80-.).*, vol. 351, no. 6268, pp. 58–62, Jan. 2016, doi: 10.1126/science.aad2688.

[9] W. Du, X. Ren, Z. Pei, and C. Ma, "Ceramic Binder Jetting Additive Manufacturing: A Literature Review on Density," *J. Manuf. Sci. Eng.*, vol. 142, no. 4, Apr. 2020, doi: 10.1115/1.4046248.

[10] S. Gopagoni *et al.*, "Microstructural evolution in laser deposited nickel-titanium-carbon in situ metal matrix composites," *J. Alloys Compd.*, vol. 509, no. 4, pp. 1255–1260, Jan. 2011, doi: 10.1016/j.jallcom.2010.09.208.

[11] D. B. Miracle, "Metal matrix composites - From science to technological significance," *Compos. Sci. Technol.*, vol. 65, no. 15-16 SPEC. ISS., pp. 2526–2540, Dec. 2005, doi: 10.1016/j.compscitech.2005.05.027.

[12] R. Galante, C. G. Figueiredo-Pina, and A. P. Serro, "Additive manufacturing of ceramics for dental applications: A review," *Dental Materials*, vol. 35, no. 6. Elsevier Inc., pp. 825–846, Jun. 01, 2019, doi: 10.1016/j.dental.2019.02.026.

[13] J. E. Nevelos, E. Ingham, C. Doyle, A. B. Nevelos, and J. Fisher, "The influence of acetabular cup angle on the wear of 'BIOLOX Forte' alumina ceramic bearing couples in a hip joint simulator," *J. Mater. Sci. Mater. Med.*, vol. 12, no. 2, pp. 141–144, 2001, doi: 10.1023/A:1008970027306.

[14] W. Höland, M. Schweiger, R. Watzke, A. Peschke, and H. Kappert, "Ceramics as biomaterials for dental restoration," *Expert Rev. Med. Devices*, vol. 5, no. 6, pp. 729–745, Nov. 2008, doi: 10.1586/17434440.5.6.729.

[15] X. He, Y. Z. Zhang, J. P. Mansell, and B. Su, "Zirconia toughened alumina ceramic foams for potential bone graft applications: Fabrication, bioactivation, and cellular responses," in *Journal of Materials Science: Materials in Medicine*, Jul. 2008, vol. 19, no. 7, pp. 2743–2749, doi: 10.1007/s10856-008-3401-x.

[16] Y. Hu and W. Cong, "A review on laser deposition-additive manufacturing of ceramics and ceramic reinforced metal matrix composites," *Ceramics International*, vol. 44, no. 17. Elsevier Ltd, pp. 20599–20612, Dec. 01, 2018, doi: 10.1016/j.ceramint.2018.08.083.

[17] W. Du, X. Ren, Y. Chen, C. Ma, M. Radovic, and Z. Pei, "Model guided mixing of ceramic powders with graded particle sizes in binder jetting additive manufacturing," in *ASME 2018 13th International Manufacturing Science and Engineering Conference, MSEC 2018*, Sep. 2018, vol. 1, doi: 10.1115/MSEC2018-6651.

[18] S. Haeri, Y. Wang, O. Ghita, and J. Sun, "Discrete element simulation and experimental study of powder spreading process in additive manufacturing," *Powder Technol.*, vol. 306, pp. 45–54, Jan. 2017, doi: 10.1016/j.powtec.2016.11.002.

[19] G. Manogharan, M. Kioko, and C. Linkous, "Binder Jetting: A Novel Solid Oxide Fuel-Cell Fabrication Process and Evaluation," *JOM*, vol. 67, no. 3, pp. 660–667, Mar. 2015, doi: 10.1007/s11837-015-1296-9.

[20] S. Shrestha and G. Manogharan, "Optimization of Binder Jetting Using Taguchi Method," *JOM*, vol. 69, no. 3, pp. 491–497, Mar. 2017, doi: 10.1007/s11837-016-2231-4.

[21] Y. Bai, G. Wagner, and C. B. Williams, "Effect of particle size distribution on powder packing and sintering in binder jetting additive manufacturing of metals," *J. Manuf. Sci. Eng. Trans. ASME*, vol. 139, no. 8, Aug. 2017, doi: 10.1115/1.4036640.

[22] H. Chen, Y. Chen, Y. Liu, Q. Wei, Y. Shi, and W. Yan, "Packing quality of powder layer during counter-rolling-type powder spreading process in additive manufacturing," *Int. J. Mach. Tools Manuf.*, vol. 153, p. 103553, Jun. 2020, doi: 10.1016/j.ijmachtools.2020.103553.

[23] H. Chen, Q. Wei, Y. Zhang, F. Chen, Y. Shi, and W. Yan, "Powder-spreading mechanisms in powder-bed-based additive manufacturing: Experiments and computational modeling," *Acta Mater.*, vol. 179, pp. 158–171, Oct. 2019, doi: 10.1016/j.actamat.2019.08.030.

[24] W. Nan, M. Pasha, and M. Ghadiri, "Numerical simulation of particle flow and segregation during roller spreading process in additive manufacturing," *Powder Technol.*, vol. 364, pp. 811–821, Mar. 2020, doi: 10.1016/j.powtec.2019.12.023.

[25] W. Nan *et al.*, "Jamming during particle spreading in additive manufacturing," *Powder Technol.*, vol. 338, pp. 253–262, Oct. 2018, doi: 10.1016/j.powtec.2018.07.030.

[26] E. J. R. Parteli and T. Pöschel, "Particle-based simulation of powder application in additive manufacturing," *Powder Technol.*, vol. 288, pp. 96–102, Jan. 2016, doi: 10.1016/j.powtec.2015.10.035.

[27] Y. Lee, A. K. Gurnon, D. Bodner, and S. Simunovic,

"Effect of Particle Spreading Dynamics on Powder Bed Quality in Metal Additive Manufacturing," *Integr. Mater. Manuf. Innov.*, vol. 9, no. 4, pp. 410–422, Dec. 2020, doi: 10.1007/s40192-020-00193-1.

[28] Y. S. Lee, P. Nandwana, and W. Zhang, "Dynamic simulation of powder packing structure for powder bed additive manufacturing," *Int. J. Adv. Manuf. Technol.*, vol. 96, no. 1–4, pp. 1507–1520, Apr. 2018, doi: 10.1007/s00170-018-1697-3.

[29] W. Du, M. Singh, and D. Singh, "Binder jetting additive manufacturing of silicon carbide ceramics: Development of bimodal powder feedstocks by modeling and experimental methods," *Ceram. Int.*, vol. 46, no. 12, pp. 19701–19707, Aug. 2020, doi: 10.1016/j.ceramint.2020.04.098.

[30] Y. Bai, G. Wagner, and C. B. Williams, "Effect of Bimodal Powder Mixture on Powder Packing Density and Sintered Density in Binder Jetting of Metals."

[31] H. Miyanaji, K. M. Rahman, M. Da, and C. B. Williams, "Effect of fine powder particles on quality of binder jetting parts," *Addit. Manuf.*, vol. 36, p. 101587, Dec. 2020, doi: 10.1016/j.addma.2020.101587.

[32] A. Mostafaei *et al.*, "Binder jet 3D printing – Process parameters, materials, properties, and challenges," *Progress in Materials Science*. Elsevier Ltd, p. 100707, Jun. 15, 2020, doi: 10.1016/j.pmatsci.2020.100707.

[33] Y. Zhang, W. Jarosinski, Y. G. Jung, and J. Zhang, "Additive manufacturing processes and equipment," in *Additive Manufacturing: Materials, Processes, Quantifications and Applications*, Elsevier, 2018, pp. 39–51.

[34] P. Lynch, C. Hasbrouck, J. Wilck, M. Kay, and G. Manogharan, "Challenges and opportunities to integrate the oldest and newest manufacturing processes: metal casting and additive manufacturing," *Rapid Prototyp. J.*, vol. 26, no. 6, pp. 1145–1154, Jun. 2020, doi: 10.1108/RPJ-10-2019-0277.

[35] D. Martinez, C. Bate, and G. Manogharan, "Towards Functionally Graded Sand Molds for Metal Casting: Engineering Thermo-mechanical Properties Using 3D Sand Printing," *JOM*, vol. 72, no. 3, pp. 1340–1354, Mar. 2020, doi: 10.1007/s11837-019-03975-x.

[36] P. King, D. Martinez, G. Manogharan, "Novel Sprue Designs to Reduce Casting Defects in Nickel-Aluminum Bronze: A Computational Study | International Manufacturing Science and Engineering Conference | ASME Digital Collection." https://asmedigitalcollection.asme.org/MSEC/proceedings-abstract/MSEC2020/84256/V001T01A054/1095646 (accessed Feb. 28, 2021).

[37] S. Cao, Y. Qiu, X. F. Wei, and H. H. Zhang, "Experimental and theoretical investigation on ultra-thin powder layering in three dimensional printing (3DP) by a novel double-smoothing mechanism," *J. Mater. Process. Technol.*, vol. 220, pp. 231–242, Jun. 2015, doi: 10.1016/j.jmatprotec.2015.01.016.

[38] "Naigai cerabeads® 60 : products - Itochu Ceratech corp." http://www.itc-cera.co.jp/english/prod/index.html (accessed Nov. 17, 2020).

[39] S. R. Sama, T. Badamo, and G. Manogharan, "Case Studies on Integrating 3D Sand-Printing Technology into the Production Portfolio of a Sand-Casting Foundry," *Int. J. Met.*, vol. 14, no. 1, pp. 12–24, Jan. 2020, doi: 10.1007/s40962-019-00340-1.

[40] M. Upadhyay, T. Sivarupan, and M. El Mansori, "3D printing for rapid sand casting—A review," *Journal of Manufacturing Processes*, vol. 29. Elsevier Ltd, pp. 211–220, Oct. 01, 2017, doi: 10.1016/j.jmapro.2017.07.017.

[41] J. Thiel, S. Ravi, and N. Bryant, "Advancements in materials for three-dimensional printing of molds and cores," *Int. J. Met.*, vol. 11, no. 1, pp. 3–13, Jan. 2017, doi: 10.1007/s40962-016-0082-y.

[42] C. Sun *et al.*, "Effect of particle size gradation on the performance of glass-ceramic 3D printing process," *Ceram. Int.*, vol. 43, no. 1, pp. 578–584, Jan. 2017, doi: 10.1016/j.ceramint.2016.09.197.

[43] J. Zheng, W. B. Carlson, and J. S. Reed, "The packing density of binary powder mixtures," *J. Eur. Ceram. Soc.*, vol. 15, no. 5, pp. 479–483, Jan. 1995, doi: 10.1016/0955-2219(95)00001-B.

[44] T. Stovall, F. de Larrard, and M. Buil, "Linear packing density model of grain mixtures," *Powder Technol.*, vol. 48, no. 1, pp. 1–12, Sep. 1986, doi: 10.1016/0032-5910(86)80058-4.

[45] J. Ge and C. A. Monroe, "The Effect of Coefficient of Restitution in Modeling of Sand Granular Flow for Core Making: Part I Free-Fall Experiment and Theory," *Int. J. Met.*, vol. 13, no. 4, pp. 753–767, Oct. 2019, doi: 10.1007/s40962-019-00333-0.

[46] A. Anand, J. S. Curtis, C. R. Wassgren, B. C. Hancock, and W. R. Ketterhagen, "Predicting discharge dynamics from a rectangular hopper using the discrete element method (DEM)," *Chem. Eng. Sci.*, vol. 63, no. 24, pp. 5821–5830, Dec. 2008, doi: 10.1016/j.ces.2008.08.015.

[47] "Coefficients of Friction between Calcareous Sands and Some Building Materials, and Their Significance." https://apps.dtic.mil/sti/citations/ADA066297 (accessed Feb. 28, 2021).

[48] C. Meier, R. Weissbach, J. Weinberg, W. A. Wall, and A. J. Hart, "Critical influences of particle size and adhesion on the powder layer uniformity in metal additive manufacturing," *J. Mater. Process. Technol.*, vol. 266, pp. 484–501, Apr. 2019, doi: 10.1016/j.jmatprotec.2018.10.037.

[49] Y. Ma, T. M. Evans, N. Philips, and N. Cunningham, "Numerical simulation of the effect of fine fraction on the flowability of powders in additive manufacturing," *Powder Technol.*, vol. 360, pp. 608–621, Jan. 2020, doi: 10.1016/j.powtec.2019.10.041.

[50] Y. Lee, S. Simunovic, and A. K. Gurnon, "Quantification of Powder Spreading Process for Metal Additive

Manufacturing," 2019. Accessed: Feb. 17, 2021. [Online]. Available: http://www.osti.gov/scitech/.
[51] B. Yan, R. A. Regueiro, and S. Sture, "Three-dimensional ellipsoidal discrete element modeling of granular materials and its coupling with finite element facets," *Eng. Comput. (Swansea, Wales)*, vol. 27, no. 4, pp. 519–550, Jan. 2010, doi: 10.1108/02644401011044603.
[52] M. Y. Shaheen, A. R. Thornton, S. Luding, and T. Weinhart, "The influence of material and process parameters on powder spreading in additive manufacturing," *Powder Technol.*, vol. 383, pp. 564–583, May 2021, doi: 10.1016/j.powtec.2021.01.058.
[53] G. Miao, W. Du, M. Moghadasi, Z. Pei, and C. Ma, "Ceramic binder jetting additive manufacturing: Effects of granulation on properties of feedstock powder and printed and sintered parts," *Addit. Manuf.*, vol. 36, p. 101542, Dec. 2020, doi: 10.1016/j.addma.2020.101542.